

1 Article

2 

# Energy-Based Design Criterion of Dissipative

  
3 

# Bracing Systems for Seismic Retrofit of Frame

  
4 

# Structures

5 **Gloria Terenzi** <sup>1\*</sup>6 <sup>1</sup> Department of Civil and Environmental Engineering, University of Florence, Italy; gloria.terenzi@unifi.it

7 \* Correspondence: gloria.terenzi@unifi.it; Tel.: +39-55-275-8887

8 **Featured Application:** An energy-based sizing criterion is proposed to help designing dissipative  
9 bracing systems incorporating fluid viscous spring-dampers for seismic retrofit of frame  
10 structures.11 **Abstract:** Direct sizing criteria represent useful tools in the design of dissipative bracing systems for  
12 the advanced seismic protection of existing frame structures, especially when incorporated dampers  
13 feature a markedly non-linear behaviour. An energy-based procedure is proposed herein to this  
14 aim, focusing attention on systems including fluid viscous devices. The procedure starts by  
15 assuming prefixed reduction factors of the most critical response parameters in current conditions,  
16 which are evaluated by means of a conventional elastic finite element analysis. Simple formulas  
17 relating the reduction factors to the equivalent viscous damping ratio of the dissipaters,  $\xi_{eq}$ , are  
18 proposed. These formulas allow calculating the  $\xi_{eq}$  values that guarantee the achievement of target  
19 factors. Finally, the energy dissipation capacity of the devices is deduced from  $\xi_{eq}$ , finalizing their  
20 sizing process. A detailed description of the procedure is presented in the article, by distinguishing  
21 the cases where the prevailing structural deficiencies are represented by poor strength of the  
22 constituting members, from the cases having excessive horizontal displacements. A demonstrative  
23 application to the retrofit design of a reinforced concrete gym building is then offered to explicate  
24 the steps of the sizing criterion in practice, as well as to evaluate the enhancement of seismic  
25 response capacities generated by the installation of the dissipative system.26 **Keywords:** energy dissipation; dissipative braces; design criteria; seismic retrofit; frame structures.  
2728 

## 1. Introduction

29 Dissipative bracing systems are increasingly adopted in anti-seismic design of new frame  
30 structures, as well as to retrofit existing ones. Several types of technologies have been implemented,  
31 capable of supplying supplemental damping and horizontal stiffness in different proportions,  
32 depending on the mechanical characteristics of dissipaters and their installation layout. By way of  
33 example, metallic yielding devices, like ADAS (Added Damping and Stiffness) components [1-2],  
34 typically provide significant contributions in terms of both properties. On the other hand, fluid  
35 viscous dissipaters, when mounted at the tip of supporting braces in parallel with the overlying beam  
36 axis [3], slightly increase the horizontal stiffness of the structural system, while supplying high  
37 additional damping.38 A further spreading of dissipative bracing technologies in the professional community strongly  
39 depends on the availability of simple and intuitive design procedures, especially concerning the  
40 preliminary sizing of dissipaters. The first methods offered in literature start from setting the desired  
41 damping ratio (i.e. the ratio of the damping coefficient to the critical damping coefficient) in the

42 fundamental mode of vibration of the structure, in the hypothesis that the relevant effective modal  
43 mass (EMM) is a predominant portion of the total seismic mass [4-8]. In general, the practical  
44 application of these methods consists in examining the response spectra at various damping ratios  
45 and choosing the value that allows constraining the maximum “global” response parameters (base  
46 shear, top lateral displacements, etc) within targeted acceptable limits. When the devices are  
47 characterized by non linear viscous properties, the same objectives can be reached by transforming  
48 relevant damping coefficients into equivalent linear viscous coefficients [9-10]. These studies have  
49 provided the basis for the design procedures of buildings incorporating passive energy dissipation  
50 systems included in ASCE 41-06 [11] and ASCE 7-10 [12] Standards.

51 Along the same conceptual line, some procedures based on the use of normative response  
52 spectra scaled by reduction factors corresponding to the damping capacity of the devices have been  
53 proposed more recently [13-14], where reference is made to damping ratio values no greater than 0.3.  
54 Other approaches use equivalent linear or non-linear static analyses to evaluate the design actions  
55 and reduce their effects through added damping [15]. All the above-mentioned procedures are  
56 conceived for substantially regular structures. Few solutions are found for problems characterized  
57 by significant irregularities in plan and/or in elevation. Among these, a method based on properly  
58 calibrated expressions of the damping ratio derived from the results of non-linear dynamic analyses  
59 is formulated in [16, 17].

60 An alternative approach is represented by an energy-based design criterion, first proposed for  
61 fluid viscous dissipaters [3, 18], and later extended to ADAS elements [19]. This criterion consists in  
62 determining the minimum damping coefficients of the devices required to assign them the capability  
63 of dissipating a prefixed fraction,  $\beta$ , of the seismic input energy,  $E_I$ , computed on each story [18, 19]  
64 or the entire structure [20]. To facilitate the choice of  $\beta$ , preferable ranges were provided for several  
65 different structural types, and checked in relation to the assumed design targets [3, 18-20]. However,  
66 as the method requires a preliminary evaluation of the seismic input energy demand on the original  
67 structure, a finite element time-history analysis must be carried out first, and  $E_I$  post-calculated from  
68 the results. Although an energy calculation can be performed with the help of commercial finite  
69 element programs by means of simple input instructions, professional engineers are not always  
70 familiar with this design approach, and may be discouraged from using it.

71 In view of this, a new procedure that bypasses this initial step by directly estimating the  
72 minimum damping capacity to be assigned to the dissipaters is proposed in this paper, where  
73 attention is focused on the retrofit design of reinforced concrete (RC) structures. The procedure starts  
74 by assuming prefixed  $\alpha$  reduction factors of the most critical response parameters in current  
75 conditions, which are evaluated by means of a conventional elastic finite element analysis. Simple  
76 formulas relating the  $\alpha$  factors to the equivalent viscous damping ratio of the dissipaters,  $\xi_{eq}$ , are  
77 proposed. These formulas allow calculating the  $\xi_{eq}$  values guaranteeing the achievement of the target  
78  $\alpha$  factors. Finally, the energy dissipation capacity of the devices is deduced from  $\xi_{eq}$ , finalizing their  
79 sizing process.

80 A detailed description of the method is presented in the next Section. A demonstrative  
81 application to the retrofit design of a RC gym building is then offered, to explicate relevant steps in  
82 practice. Finally, a performance assessment analysis of the structure in original and retrofitted  
83 conditions is carried out to evaluate the enhancement of seismic response capacities produced by the  
84 incorporation of the dissipative bracing system.

85 **2. Design Procedure**

86 The design procedure is based on the assumption that for relatively stiff structures, i.e. with  
87 fundamental translational vibration period in current conditions,  $T_1^{cs}$ , below 0.8 s, a substantial  
88 improvement of seismic performance can be reached by incorporating a supplemental damping  
89 system with limited stiffening capacity. For structures with a greater fundamental translational  
90 period, a supplemental stiffness contribution helps control lateral displacements better, which  
91 prevents an over-dissipation demand to the damping technology adopted.

92 In the following, attention is focused on the first class of structures, where the retrofit design  
93 objectives can be met by the added damping, with a marginal role of supplemental stiffness. This  
94 prompts to select bracing systems that incorporate pressurized FV spring-dampers as protective  
95 strategy. Indeed, the spring component of the devices, acting in-series with the steel braces,  
96 remarkably constrains the total horizontal translational stiffness of these systems. This results in a  
97 moderate contribution (normally below 10%) to the lateral stiffness of the retrofitted structures.

98 The  $\alpha$  reduction factors are calibrated on the mechanical characteristics of this type of devices.  
99 For dampers adding a non negligible supplemental stiffness, the procedure follows the same steps,  
100 but different criteria for the evaluation of  $\alpha$  are required, which will be detailed in a further step of  
101 this research.

102 In view of the practical application of the design method, a distinction is made between the cases  
103 where the prevailing structural deficiencies are represented by poor shear or bending moment  
104 strength of columns and/or beams — where  $\alpha$  is intended as “stress-related” reduction factor, named  
105  $\alpha_s$  in the following — and the cases having excessive horizontal displacements, where  $\alpha$  is intended  
106 as “deformation-related” reduction factor,  $\alpha_d$ .

107 *2.1. Structures with Poor Shear or Bending Moment Strength of Constituting Members*

108 The basic design objective of supplemental damping-based retrofit interventions is always a  
109 significant enhancement of seismic performance as compared to the original structural conditions.  
110 When high-damping capacity dissipaters are adopted, like pressurized FV devices, the attainment of  
111 the Immediate Occupancy (IO) seismic performance level can be planned up to the maximum  
112 considered earthquake (MCE), with reasonable costs and architectural impact. This objective  
113 corresponds to keep the response of the structural members within the elastic field, thus replacing  
114 the plastic demand in current conditions with the dissipative action of the protective system. The  
115 design procedure is based on this target, and articulated in the four steps described below.

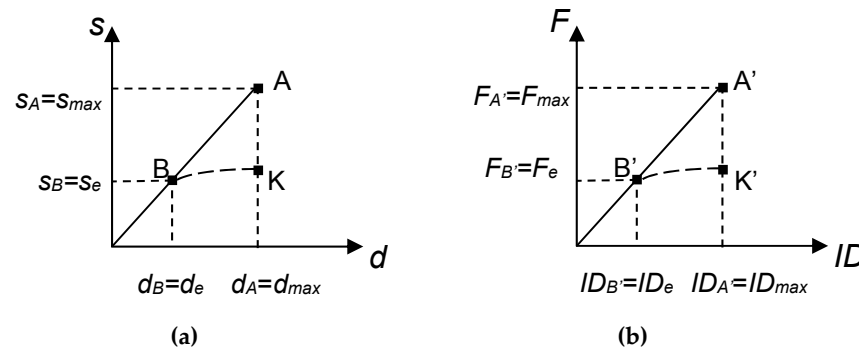
116 1. Development of an elastic finite element verification analysis and relevant stress state checks in  
117 current conditions.

118 The shear and bending moment-related stress states in columns and beams are calculated by  
119 means of an elastic finite element (either modal superposition with response spectrum or time-  
120 history) analysis of the structure in current conditions. Then, the maximum stress states are checked  
121 by comparison with the corresponding elastic limit values for the two axes in plan of the reference  
122 Cartesian coordinate system, X and Y (Z being the vertical axis). The shear and bending moment  
123 values in the member that proves to be subjected to the highest unsafe stress conditions are named

124  $V_{j,c}^a$  and  $M_{j,c}^a$ , where index  $j$  refers to the axis ( $j=X,Y$ ),  $c$  denotes the “critical” member(s), and  $a$   
 125 means that the values are derived from the elastic assessment analysis.

126 2. Evaluation of the target stress reduction factors,  $\alpha_s$ .

127 This evaluation is carried out by referring to the scheme in Figure 1a, where  $d, s$  represent general  
 128 deformation-related and stress-related parameters for the critical member(s). The objective of the  
 129 retrofit design consists in reducing the seismic demand in current state calculated by the elastic  
 130 analysis in step 1 — denoted by point A with coordinates  $(d_A=d_{max}, s_A=s_{max})$ , where  $d_{max}, s_{max}$  are the  
 131 maximum  $d$  and  $s$  computed values — below point B with coordinates  $(d_B=d_e, s_B=s_e)$ , where  $d_e, s_e$  are  
 132 the elastic limit deformation-related and stress-related parameters for the critical member(s),  
 133 respectively. On the contrary, in a traditional design approach the reduction of the force-related  
 134 parameter is pursued by exploiting the ductile plastic response of the structural members, by moving  
 135 the maximum response point from A to K, with coordinates  $(d_A, s_B)$ .



141 **Figure 1.** Schematic response of the critical structural member (a) and the frame structure storey to which  
 142 it belongs (b).

144 Hence, the force reduction factor,  $\alpha_s$ , targeted to reach an elastic response of the critical member  
 145 (and thus of all remaining members) when passing from original to retrofitted conditions, is given  
 146 by:

$$147 \quad \alpha_s = \frac{s_A}{s_B} \quad (1)$$

148 The  $s_A$  and  $s_B$  parameters in Figure 1 are detailed below according to the specific lack of strength  
 149 affecting the structural members in original conditions.

150 2.a. Lack of shear strength.

151 In this hypothesis,  $s_A$  is the shear force in the critical member,  $V_{j,c}^a$ , according with the notation  
 152 introduced in step 1. Said  $V_{j,c}^e = s_B$  the elastic limit shear of this member,  $\alpha_s$  — specified in this  
 153 hypothesis as  $\alpha_{Vj}$  — is evaluated as follows:

154 
$$\alpha_s = \alpha_{Vj} = \frac{s_A}{s_B} = \frac{V_{j,c}^a}{V_{j,c}^e} \quad (2)$$

155 2.b. Lack of bending moment strength.

156 Similarly to point 2.a, when the critical stress-related parameter  $s_A$  is the bending moment  $M_{j,c}^a$   
 157 (associated with the concurrent axial force,  $N_c$ , if the critical member is a column), said  $M_{j,c}^e = s_B$  the  
 158 corresponding elastic limit moment, the reduction factor  $\alpha_s$  — denoted with symbol  $\alpha_{Mj}$  in this  
 159 case — is given by:

160 
$$\alpha_s = \alpha_{Mj} = \frac{s_A}{s_B} = \frac{M_{j,c}^a}{M_{j,c}^e} \quad (3)$$

161 2.c. Passage from member to storey ( $\alpha_s \rightarrow \alpha_F$ ).

162 The A→B transition in the most critical member, governed by factor  $\alpha_{Vj}$  or  $\alpha_{Mj}$ , implies a  
 163 similar shift in the response of the frame structure storey to which the member belongs. This is  
 164 visualized in the graph of Figure 1b, where the storey shear,  $F$ , and the inter-storey drift,  $ID$ , are  
 165 assumed as response parameters, and the member response points A and B are replaced by the  
 166 corresponding storey response points A', with coordinates ( $F_A=F_{max}$ ,  $ID_A=ID_{max}$ ) and B', with  
 167 coordinates ( $F_B=F_e$ ,  $ID_B=ID_e$ ), where indexes "max" and "e" denote the maximum response value and  
 168 the corresponding elastic limit in this case too. Based on this correlation, the storey response points  
 169 A', B' in Figure 1b are reached when the critical member attains points A, B in Figure 1a. Therefore,  
 170 the reduction factor at the storey level,  $\alpha_F$ :

171 
$$\alpha_F = \frac{F_{A'}}{F_{B'}} \quad (4)$$

172 coincides with  $\alpha_{Vj}$  or  $\alpha_{Mj}$ , depending on the lack of strength assessed in the most critical member.

173 3. Correlation of  $\alpha_F$  to the dissipated energy,  $E_D$ , and the equivalent viscous damping ratio,  $\xi_{eq}$ , of  
 174 the spring-dampers.

175 The correlation is established consistently with the design objective of reducing storey response  
 176 from point A' to point B', thanks to the incorporation of the protective system. The sizing of the  
 177 dissipaters is performed first by evaluating their equivalent viscous damping ratio,  $\xi_{eq}$ , using the  
 178 general expression:

179 
$$\xi_{eq} = \frac{E_D}{4\pi E_e} \quad (5)$$

180 where  $E_D$  is the energy dissipated by the set of FV spring-dampers installed on the storey containing  
 181 the critical member, and  $E_e$  is the strain energy of the system estimated by referring to the global  
 182 response cycle of the set of devices, schematically drawn in Figure 2. Therein,  $d_{dmax}$  is the maximum  
 183 displacement,  $F_D$  is the damping force component,  $F_e$  is the elastic reaction force, and  $F_{ed} = F_e + F_D$   
 184 is the total reaction force.

185

186

187

188

189

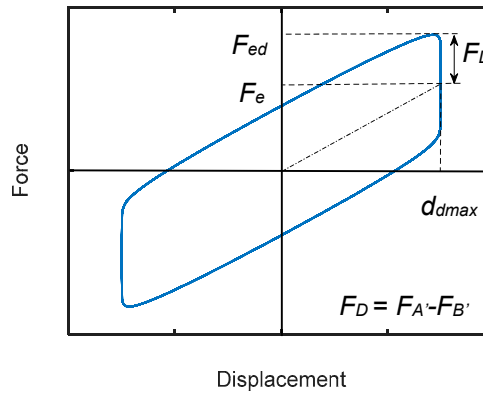
190

191

192

193

194



195

196

**Figure 2.** Schematic response cycle of the set of FV spring-dampers installed on a storey and parameters for evaluating  $\xi_{eq}$ .

197

198

In order to meet the design objective of passing from point A' to point B',  $F_D$  is set as equal to the difference between  $F_{A'}$  and  $F_{B'}$ :

199

$$F_D = F_{A'} - F_{B'} \quad (6)$$

200

201

202

In doing so, the reduction of storey response is totally assigned to the dissipative action of the protective system, as planned by this retrofit strategy. Substituting (4) in (6), the following  $F_D$  expression is obtained:

203

$$F_D = F_{A'} - F_{B'} = \alpha_F F_{B'} - F_{B'} = F_{B'}(\alpha_F - 1) \quad (7)$$

204

from which it follows:

205

$$F_{B'} = \frac{F_D}{(\alpha_F - 1)} \quad (8)$$

206

207

The  $F_e$  elastic force component is set as equal to the elastic limit value of the storey shear,  $F_{B'}$ . Therefore,  $F_{ed}$  can be alternatively expressed as a function either of  $F_D$ :

208

$$F_{ed} = F_e + F_D = F_{B'} + F_D = \frac{F_D}{(\alpha_F - 1)} + F_D = F_D \frac{\alpha_F}{(\alpha_F - 1)} \quad (9)$$

209

or of  $F_e$ , substituting (8) in (9):

210

$$F_{ed} = \alpha_F F_e \quad (10)$$

211 By referring to the response cycle in Figure 2 and relevant parameters, the following expressions  
 212 of  $E_D$  and  $E_e$  are derived:

213  $E_D = 4F_D d_{dmax}$  (11)

214  $E_e = F_{ed} d_{dmax} / 2$  (12)

215 Substituting (11) and (12) in (5), the following  $\xi_{eq}$  expression is deduced:

216  $\xi_{eq} = \frac{4F_D d_{dmax}}{4\pi(F_{ed} d_{dmax} / 2)}$  (13)

217 Introducing (8) and (9), (13) becomes:

218  $\xi_{eq} = \frac{2(\alpha_F - 1)}{\pi \alpha_F}$  (14)

219 which allows directly quantifying the equivalent viscous damping ratio demanded to obtain the  
 220 targeted elastic response up to the MCE, simply as a function of the reduction factor  $\alpha_F$ . Moreover,  
 221 by solving (5) to express  $E_D$  as a function of  $\xi_{eq}$  and considering (10), the following relation is obtained:

222  $E_D(\alpha_F) = 4\pi E_e \xi_{eq}(\alpha_F) = 4\pi(F_{ed} d_{dmax} / 2) \xi_{eq}(\alpha_F) = 2\pi \alpha_F F_e \xi_{eq}(\alpha_F) d_{dmax}$  (15)

223 4. Evaluation of the energy dissipation capacity of the dissipaters,  $E_D$ , and selection of the devices  
 224 with the nearest mechanical characteristics.

225 The basic design objective of reaching an elastic response of the most critical member(s), and  
 226 thus of relevant storey, implies that the maximum storey drift in retrofitted conditions,  $ID_{max}$ , is  
 227 constrained below the corresponding elastic limit  $ID_B = ID_e$  displayed in Figure 1b.  $ID_{max}$  is given by  
 228 the sum of  $d_{dmax}$  and the interstorey drift contribution provided by the braced structure. The latter is  
 229 normally small, because relatively stiff structures — i.e. with  $T_1^{cs}$  below about 0.8 s — are dealt with,  
 230 as mentioned above, and also because the bracing system produces in any case a stiffening effect,  
 231 although limited by the special installation layout of the FV spring-dampers. In view of this, in order  
 232 to quickly pre-estimate the energy dissipation capacity of the devices, which is a function of  $d_{dmax}$  —  
 233 other than of  $F_D$  —  $d_{dmax}$  is set as equal to  $ID_e$  at this stage. Based on this assumption, the energy  
 234 dissipation capacity to be assigned to the FV devices on the considered storey is drawn from (11):

235  $E_D = 4F_D ID_e$  (16)

236 In order to express  $E_D$  as a function of structure-related terms only, (8) is substituted in (16), and  
 237 gives:

238  $E_D(\alpha_F) = 4F_e(\alpha_F - 1)ID_e$  (17)

239 Relation (15) can be equivalently adopted to this aim:

240 
$$E_D(\alpha_F) = 2\pi\alpha_F F_e \xi_{eq}(\alpha_F) ID_e \quad (18)$$

241 The sizing process of the spring-dampers is concluded — for each storey — by selecting from  
242 the manufacturer's catalogue [21] the device with the nearest energy dissipation capacity to the  $E_D$   
243 value estimated by (17) or (18), and a stroke approximately equal to  $ID_e$ .

244 *2.2 Structures with Excessive Inter-Storey Drifts*

245 The attainment of an elastic structural response up to the MCE is assumed as the basic design  
246 objective also when the poorest response capacity is in terms of storey drifts. This is more likely  
247 verified in structures with translational period  $T_1^{cs}$  next to the 0.8 s value approximately fixed as  
248 upper limit for the application of the procedure. The design objective is reached by reducing the  
249 maximum inter-storey drift computed in current conditions, identified by  $ID_A = ID_{max}$  in Figure 1b, to  
250 the corresponding elastic limit  $ID_B = ID_e$ , i.e. scaling the drift response by a deformation-related  
251 reduction factor,  $\alpha_d$ :

252 
$$\alpha_d = \frac{ID_{A'}}{ID_{B'}} = \frac{ID_{max}}{ID_e} \quad (19)$$

253 When an elastic finite element assessment analysis is carried out on the original structure,  $\alpha_d$  is  
254 proportional to  $\alpha_F$ . For cases where an inelastic evaluation analysis is developed, assuming a typical  
255 degrading strength and degrading stiffness post-elastic behaviour — like the one qualitatively  
256 schematized by curve B'-K' in Figure 1b —  $\alpha_d$  significantly differs from  $\alpha_F$ . Therefore, the expressions  
257 of  $E_D$  and  $\xi_{eq}$  must be reformulated as a function of  $\alpha_d$ , to allow quickly estimating both quantities  
258 also for the structures where inter-storey drift is the critical response parameter.

259 Starting from relation (13), the two changes introduced as compared to Section 2.1 consist in  
260 assuming  $d_{dmax} = ID_A - ID_B = ID_{max} - ID_e$ , and  $F_{ed} = F_K = F_D$ . The first assumption corresponds to assign the  
261 dampers the capacity of absorbing the post-elastic displacement demand of the structure computed  
262 in original conditions, so as to meet the design objective of limiting its response to the elastic field,  
263 after retrofit. The second assumption derives from the fact that the displacement performance  
264 enhancement must be achieved essentially by means of the dissipative capacity of the FV devices, by  
265 neglecting at the sizing stage the slight stiffening effects related to their elastic spring function. Then,  
266 according to (19), the following  $\xi_{eq}$  expression is obtained:

267 
$$\xi_{eq}(\alpha_d) = \frac{4F_D(ID_{A'} - ID_{B'})}{4\pi(F_{ed}ID_e/2)} = \frac{4F_D(ID_{max} - ID_e)}{4\pi(F_{ed}ID_e/2)} = \frac{2}{\pi}(\alpha_d - 1) \quad (20)$$

268 By referring to (13), the corresponding energy dissipation capacity to be assigned to the dampers  
269 on the considered storey results as follows:

270 
$$E_D(\alpha_d) = 2\pi F_e \xi_{eq}(\alpha_d) ID_e \quad (21)$$

271        Similarly to the case of poor strength of members, the tentative design choice of the device is  
272        carried out by referring to the spring-damper with the nearest energy dissipation capacity to  $E_D$ ,  
273        estimated by (20), and stroke equal to  $(ID_{max}-ID_e)$ .

274        **3. Geometrical and Structural Characteristics of the Case Study Building**

275        The case study examined for a first demonstrative application of the design criterion is the gym  
276        in a school in Florence, built in 1971, two external views and an internal view of which are displayed  
277        in Figure 3. Figures 4 and 5 show the structural plan and the transversal cross section, respectively.  
278        The reference Cartesian coordinate system assumed in the analyses is indicated in Figures 4 and 5  
279        too. As highlighted in Figure 4, the plan is rectangular, with sides of 14.4 m in transversal direction,  
280        parallel to X, and 24.25 m in longitudinal direction, parallel to Y. The height of the roof top is equal  
281        to 9.17 m, whereas the height of the façades, measured on top of the end section of the roof beams, is  
282        equal to 8.67 m. The structure is constituted by 9 identical RC frames of two columns each, numbered  
283        C1-C2 through C17-C18 in Figure 4, placed at a mutual distance of 3 m. The cross sections of beams  
284        and columns and relevant reinforcement details, redrawn from the original structural design  
285        drawings, are illustrated in Figure 6.

286

287



294        (a)



295        (b)



296        (c)

297        **Figure 3.** Lateral (a), front (b) and internal (c) views of the building.

296

297

298  
299  
300  
301  
302  
303  
304  
305  
306  
307  
308  
309  
310  
311  
312  
313  
314  
315  
316

318  
319  
320  
321  
322  
323  
324  
325  
326  
327  
328  
329  
330  
331  
332  
333

334  
335  
336  
337

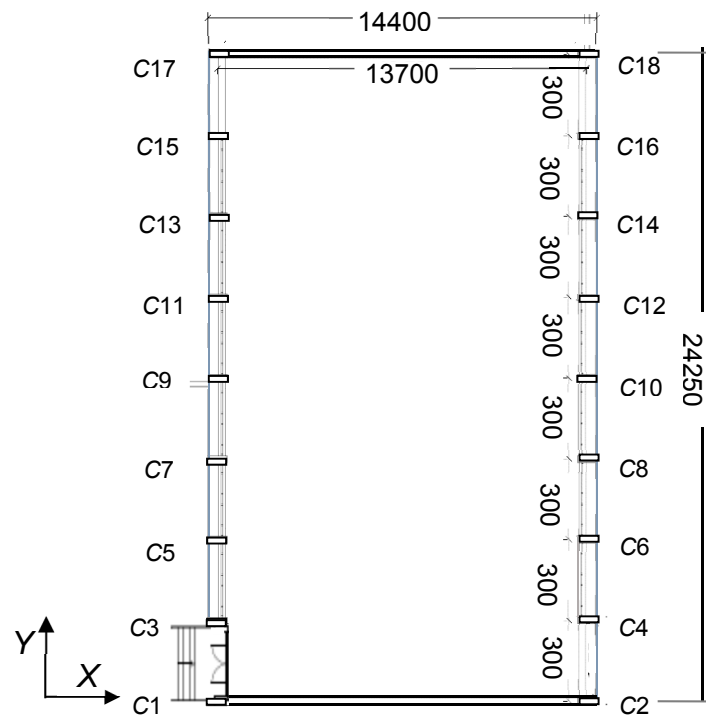


**Figure 4.** Structural plan of the building (dimensions in millimeters)

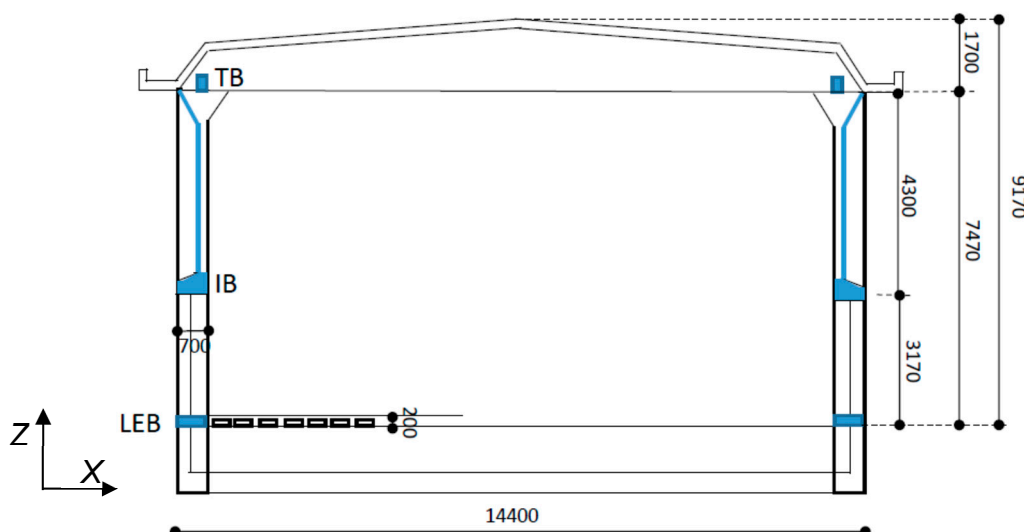
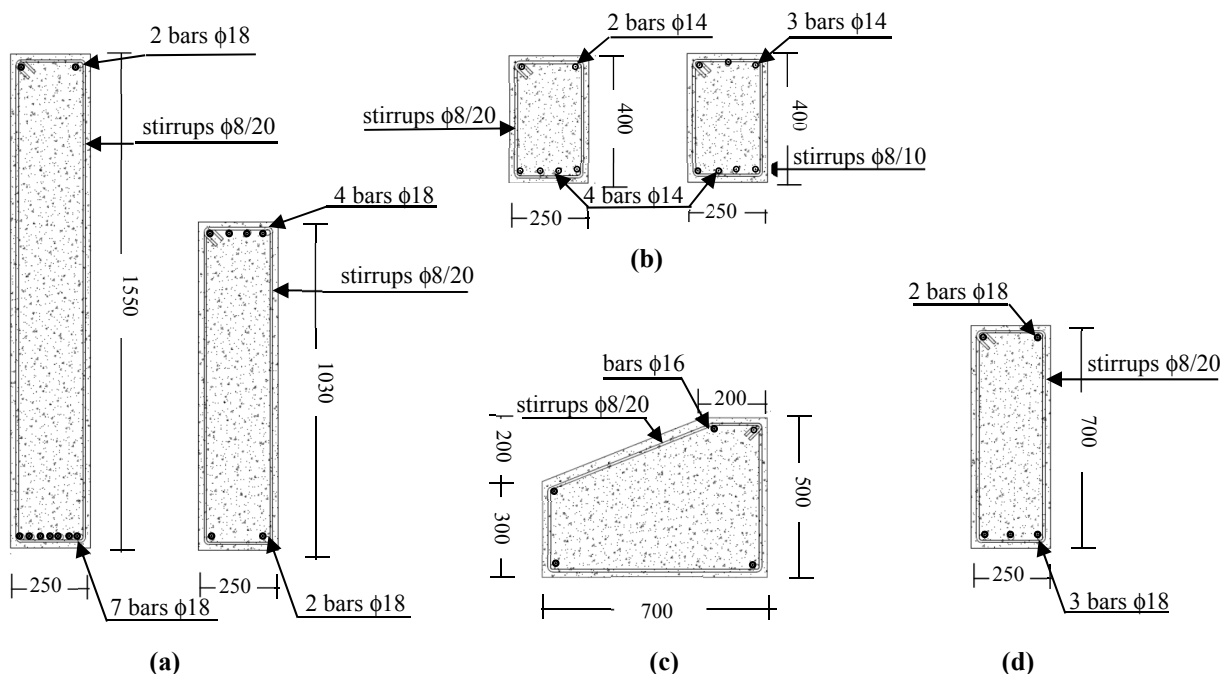


**Figure 5.** Cross section of the building (dimensions in millimeters).

338

339



340

341

342

343

344

345

346

347

348

349

350

351

352

353

354

355

**Figure 6.** Redrawn cross sections of: (a) roof beams – half-span and ends; (b) top longitudinal beams TB – half-span and ends; (c) intermediate longitudinal beams IB; and (d) columns (dimensions in millimeters).

356

Columns have a mutual rectangular section with sides of 700 mm along X and 250 mm along Y.

357

Roof beams have rectangular section with base of 250 mm and height varying from 1030 mm, at the ends, to 1540 mm, at half-span. In longitudinal direction the columns are connected on top by a rectangular beam, named TB in Figure 5, with dimensions 250×400 mm×mm; at a height of 3.17 m by an intermediate beam, named IB, having a polygonal section with base of 700 mm and maximum lateral side of 500 mm; and at the base by a rectangular beam constituting the lateral edge beam of the ground floor, named LEB, with dimensions 200×700 mm×mm. The IB beam, which supports the curtain wall-type glazed portions of the façades, subdivides all columns in two levels along the height.

358

The structure of the roof floor is 160 mm thick and made of 120 mm-high and 100 mm-wide partly prefabricated RC joists, parallel to Y and placed at a mutual distance of 400 mm; clay lug bricks; and a 40 mm thick upper RC slab. The ground floor only differs for the height of the joists, equal to 160 mm, which determines a total thickness of 200 mm. The foundation consists of a 400 mm-thick continuous slab, with 1400 mm-high (slab thickness included) and 250 mm-wide transversal rib beams, which connect the column base sections in X direction and support the ground floor.

359

A selective investigation campaign was carried out on materials and structural members, including on-site Son-Reb, pacometric and Vickers-type micro-durometer analyses, and laboratory tests on concrete and steel bar samples. Based on the prescriptions of Italian Standards [22, 23], as well as on professional protocols [24, 25], the tests met the basic knowledge level (named LC1 in [22]) for the structural assessment analysis of public buildings in Italy. The corresponding value of the confidence factor, i.e. the additional knowledge level-related safety coefficient to be introduced in stress state checks, is equal to 1.35. The following main properties resulted from the characterization tests: mean cubic compressive strength of concrete equal to 19.6 N/mm<sup>2</sup>; yield stress and limit stress of steel equal to 417 MPa and 594 MPa, respectively.

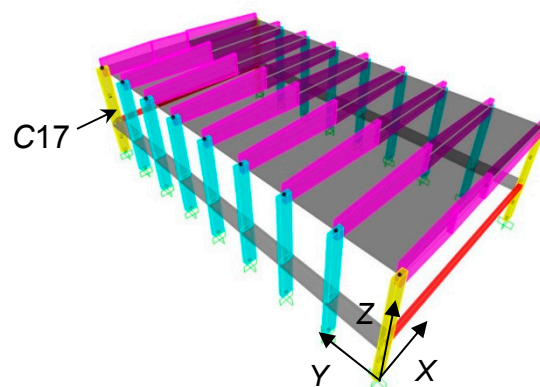
380 **4. Verification Analysis in Current Conditions (Step 1 of the Design Procedure)**

381 The verification enquiry in current conditions, constituting Step 1 of the design procedure, is  
 382 articulated in a modal analysis, to calculate the vibration periods and associated modal masses, and  
 383 a time-history analysis, to assess the seismic performance in terms of stress states and displacements.

384 **4.1 Modal Analysis**

385 The finite element model of the structure, a perspective view of which is displayed in Figure 7,  
 386 was generated by SAP2000NL calculus program [26] using frame type elements for all structural  
 387 members. The modal analysis carried out by the model shows two first horizontal translational  
 388 modes along *X* and *Y*, with vibration periods of 0.89 s (*Y*) and 0.35 s (*X*), respectively, and effective  
 389 modal mass (EMM) equal to 79% along *Y* and 88.1% along *X*. The fourth and fifth mode are  
 390 translational along *X* and *Y* too, with periods of 0.26 s (*Y*) and 0.11 s (*X*), and EMM equal to 20.9% (*Y*)  
 391 and 11.8% (*X*), which provide summed modal masses with the corresponding first mode-related  
 392 EMMs nearly equal to 100%, along both axes. The third and sixth mode are purely rotational around  
 393 the vertical axis *Z*, with periods of 0.34 s and 0.04 s, and EMM equal to 84.4% and 12.4%, giving a  
 394 summed modal mass of 96.8%.

395 The modal parameters quantitatively confirm a notably different translational behaviour of the  
 396 structure along the two directions in plan, as a consequence of the markedly different sides of  
 397 columns along *X* and *Y*, and the much higher flexural stiffness of the roof beams in comparison to  
 398 the longitudinal beams.

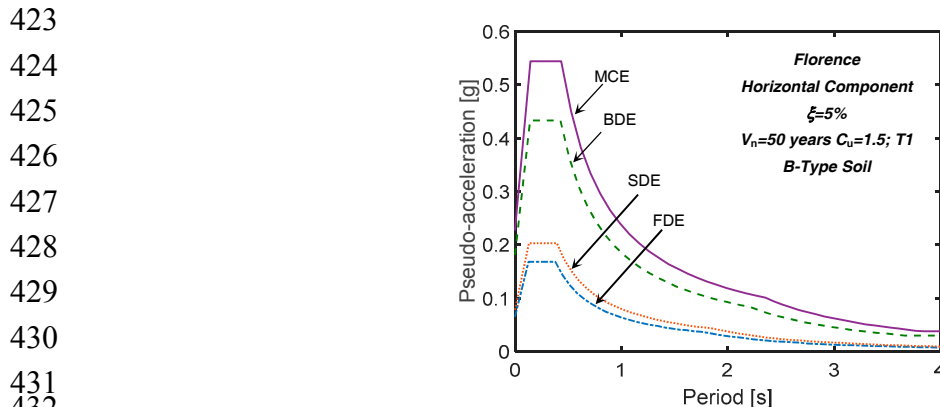


409 **Figure 7.** View and reference coordinate system of the finite element model.

410 **4.2 Time-History Verification and Performance Assessment Analysis**

411 The performance evaluation enquiry was carried out for the four reference seismic levels fixed  
 412 in the Italian Standards [23], that is, Frequent Design Earthquake (FDE, with 81% probability of being  
 413 exceeded over the reference time period  $V_R$ ); Serviceability Design Earthquake (SDE, with 50%/ $V_R$   
 414 probability); Basic Design Earthquake (BDE, with 10%/ $V_R$  probability); and Maximum Considered  
 415 Earthquake (MCE, with 5%/ $V_R$  probability). The  $V_R$  period is fixed at 75 years, which is obtained by  
 416 multiplying the nominal structural life  $V_N$  of 50 years by a coefficient of use  $C_u$  equal to 1.5, imposed  
 417 to structures whose seismic resistance is of importance in view of the consequences associated with  
 418 their possible collapse, like the case study school gym building. By referring to topographic category  
 419 T1 (flat surface), and B-type soil, the resulting peak ground accelerations for the four seismic levels  
 420 referred to the city of Florence are as follows: 0.065 g (FDE), 0.078 g (SDE), 0.181 g (BDE), and 0.227 g

421 (MCE). Relevant pseudo-acceleration elastic response spectra at linear viscous damping ratio  $\xi=5\%$   
 422 are plotted in Figure 8.



433 **Figure 8.** Normative pseudo-acceleration elastic response spectra for Florence.

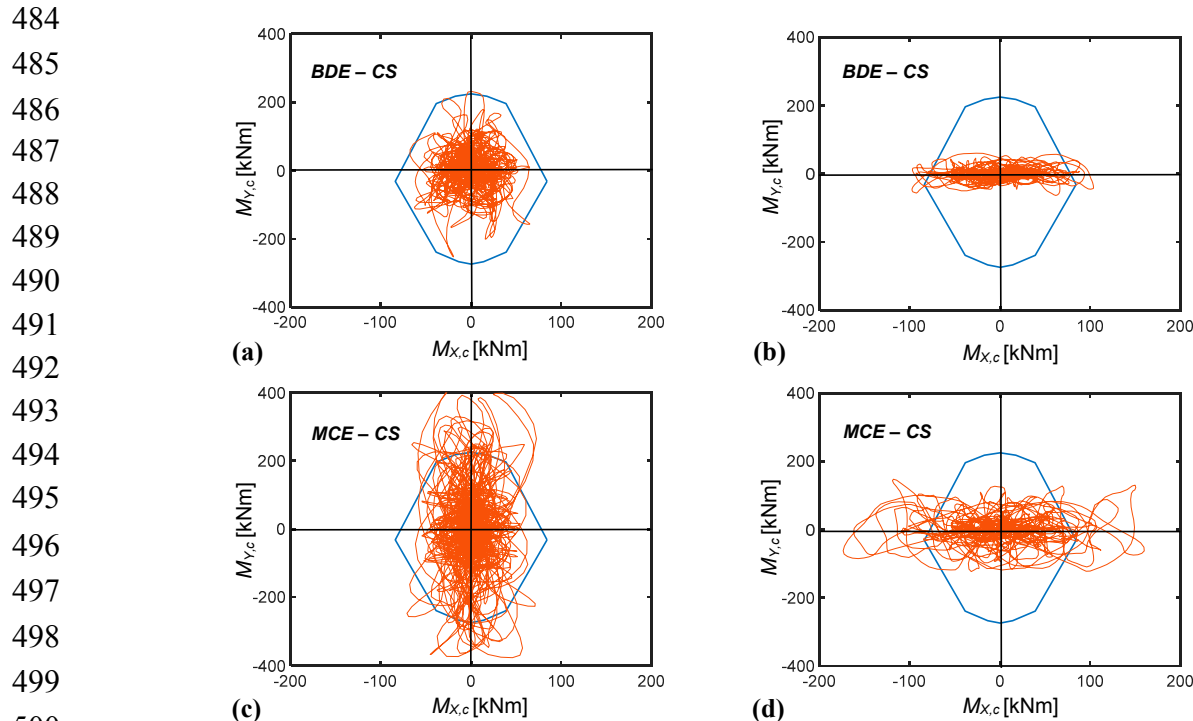
434 Time-history analyses were developed by assuming artificial ground motions as inputs,  
 435 generated in families of seven by SIMQKE-II software [27] from the spectra above. As required by  
 436 the Italian Standards [22], as well as by several other international seismic Codes and Regulations  
 437 [11,28], in each time-history analysis the accelerograms were assumed in groups of two simultaneous  
 438 horizontal components, with the first one selected from the first generated family of seven motions,  
 439 and the second one selected from the second family.

440 The results of the analyses carried out at the FDE and the SDE are evaluated in terms of inter-  
 441 level drift ratio (i.e. the ratio of inter-level drift to inter-level height of columns),  $ILD_r$ , which is  
 442 equivalent to the inter-storey drift ratio in the presence of a system of continuous intermediate beams,  
 443 although without a floor. The maximum  $ILD_r$  values induced by the most severe among the seven  
 444 groups of input motions,  $ILD_{r,max}$ , are as follows: 0.07% (FDE), 0.09% (SDE) in X, and 0.06% (FDE),  
 445 0.07% (SDE) in Y, on the first level; and 0.13% (FDE), 0.16% (SDE) in X, and 0.53% (FDE), 0.64% (SDE)  
 446 in Y, on the second level. The drift ratios in X are far below the 0.33% limitation adopted by [23] at  
 447 the Operational (OP) performance level for frame structures interacting with drift-sensitive non-  
 448 structural elements, like the masonry infills on the first level and the curtain wall-type windows on  
 449 the second level, for the main façades of the building, and the infills situated on both levels, for the  
 450 side façades. The  $ILD_{r,max}$  values obtained at the second level in Y are 1.6 times (FDE) and about twice  
 451 (SDE) the OP-related limit, and also greater than the drift threshold adopted by [23] for the Immediate  
 452 Occupancy (IO) performance level, equal to 0.5%.

453 The  $ILD_{r,max}$  values computed for the second level in Y are equal to 1.36% at the BDE, and 1.69%  
 454 at the MCE, assessing moderate (BDE) to high (MCE) potential plastic demands on columns — should  
 455 an inelastic finite element analysis be carried out —, and severe (BDE) to very severe (MCE) damage  
 456 of infills and curtain-wall windows. Consequently, the performance level attained in terms of  
 457 displacement response is Life Safety (LS), both for the BDE and the MCE. At the same time,  $ILD_{r,max}$   
 458 is no greater than 0.18% (BDE) and 0.22% (MCE) on the first level in Y, i.e. only 13% of the second  
 459 level values. This identifies a cantilever-like response of the structure along Y, with structural and  
 460 non-structural damage located on the second level. As discussed in the following Sections, this  
 461 suggests to incorporate the dissipaters on the upper level only, in order to adequately exploit their  
 462 damping capacity, and limit the cost of the retrofit intervention. In X direction  $ILD_{r,max}$  is equal to 0.2%  
 463 (BDE), 0.25% (MCE) on the first level, and 0.36% (BDE), 0.45% (MCE) on the second level. The inter-

464 level drift profile depicts a frame-like layout along this axis, which approaches a shear-type shape on  
 465 the second level, as a consequence of the high flexural stiffness of the roof beams in the X-Z vertical  
 466 plan (which determines nearly a sliding-clamped constraint condition on the top section of columns).

467 The BDE and MCE-related response was assessed also in terms of stress levels. The shear-related  
 468 checks are met in both directions and for both levels, up to the MCE. On the other hand, the combined  
 469 axial force-biaxial bending moment stress state checks are met only for the internal columns (C3  
 470 through C16, according to the numbering in Figure 4) on the first level at the BDE. The response of  
 471 corner columns (C1, C2, C17 and C18) at this level, as well as of all columns on the second level is  
 472 unsafe starting from the BDE. By way of example, the  $M_{x,c}$ - $M_{y,c}$  biaxial moment interaction curves  
 473 (being  $M_{x,c}$ ,  $M_{y,c}$  the bending moments around the X and Y axes) graphed by jointly plotting the two  
 474 bending moment response histories obtained from the most demanding among the seven groups of  
 475 MCE-scaled accelerograms, are plotted in Figure 9 for a corner column, namely C17. The boundary  
 476 of the  $M_{x,c}$ - $M_{y,c}$  elastic interaction domain traced out for the value of the axial force referred to the  
 477 basic combination of gravity loads, i.e.  $N_c=104$  kN for the corner columns, is also shown in the two  
 478 graphs. The response curves relevant to the first level highlight maximum  $M_{x,c}$ - $M_{y,c}$  combined values  
 479 slightly exceeding the safe domain boundary, at the BDE, and 1.77 times greater than the  
 480 corresponding values situated on the boundary, with prevailing contribution of  $M_{y,c}$ , at the MCE. The  
 481 curves traced out for the second level show more marked unsafe conditions at the BDE, as compared  
 482 to the first level ones, and exceed the boundary by a factor equal to 2.07, at the MCE, but with inverted  
 483 role of the moments (i.e. with prevailing contribution of  $M_{x,c}$ , for the second level).



501 **Figure 9.** Current state (CS).  $M_{x,c}$ - $M_{y,c}$  biaxial moment interaction curves at the base section of column C17  
 502 on first level (a, c) and second level (b, d) obtained from the most demanding BDE-scaled (a, b) and MCE-  
 503 scaled (c, d) group of accelerograms.

505 **5. Dissipative Bracing Retrofit Solution**506 *5.1 Characteristics of the Protective System*

507 Fluid viscous devices are among the most widely used types of rate-dependent passive energy  
 508 dampers installed in dissipative bracing technologies worldwide. This is owed to their high damping  
 509 capacities, stable mechanical properties over time, simple installation procedures, limited  
 510 architectural and visual impact, competitive costs and, in the case of pressurized elements, inherent  
 511 self-centering qualities [29-32].

512 Within this class, a special type of pressurized FV devices has been studied for several years by  
 513 the author and co-authors, focusing attention on their mechanical characterization, the  
 514 implementation of analytical and numerical models to simulate their dynamic response, the  
 515 formulation of sizing and design criteria, and the application to several different protective  
 516 technologies and structural typologies. Concerning their analytical modelling, the time-dependent  
 517  $F_D$  damping and  $F_{ne}$  non-linear elastic reaction forces corresponding to the damper and spring  
 518 functions are effectively simulated by the following expressions [29, 31]:

519 
$$F_D(t) = c \text{sgn}[\dot{x}(t)] |\dot{x}(t)|^\gamma \quad (22)$$

520 
$$F_{ne}(t) = k_2 x(t) + \frac{(k_1 - k_2)x(t)}{\left[1 + \left|\frac{k_1 x(t)}{F_0}\right|^5\right]^{1/5}} \quad (23)$$

521 where  $t$ =time variable;  $c$ =damping coefficient;  $\text{sgn}(\cdot)$ =signum function;  $\dot{x}(t)$  =device velocity;  
 522  $|\cdot|$ =absolute value;  $\gamma$ =fractional exponent, ranging from 0.1 to 0.2;  $F_0$ =static pre-load force;  $k_1$ ,  
 523  $k_2$ =stiffness of the response branches situated below and beyond  $F_0$ ; and  $x(t)$ =device displacement.  
 524 For the development of the numerical analyses, the finite element model of a FV spring-damper is  
 525 obtained by combining in parallel a non-linear dashpot and a non-linear spring with reaction forces  
 526 given by expressions (22) and (23), respectively. Both types of elements are currently incorporated in  
 527 commercial structural analysis programs, such as the SAP2000NL code used in this study.

528 The installation layout of the springs-dampers in the dissipative bracing system is illustrated by  
 529 the drawing in Figure 10, referred to the case study building, and corresponding to the basic  
 530 configuration devised for RC frame buildings. Therein, a pair of interfaced devices is placed in  
 531 parallel with the connecting beam axis at the tip of each couple of supporting braces. A half-stroke  
 532 initial position is imposed on site to the pistons of both spring-dampers, so as to obtain symmetrical  
 533 tension-compression response cycles — like the one traced out in the scheme of Figure 2 — starting  
 534 from a compressive-only response of the single devices. This position is obtained during the assembly  
 535 operations by acting on a pair of threaded steel bars crossing the interfacing plate of each device, and  
 536 connected to two other bored plates, screwed into the external casing of the spring-dampers.

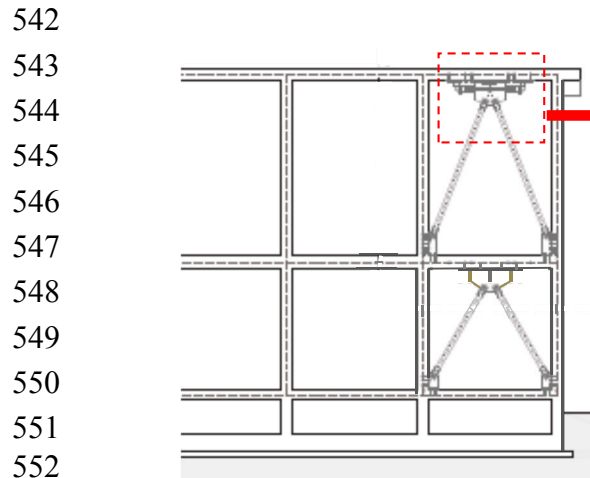
537

538

539

540

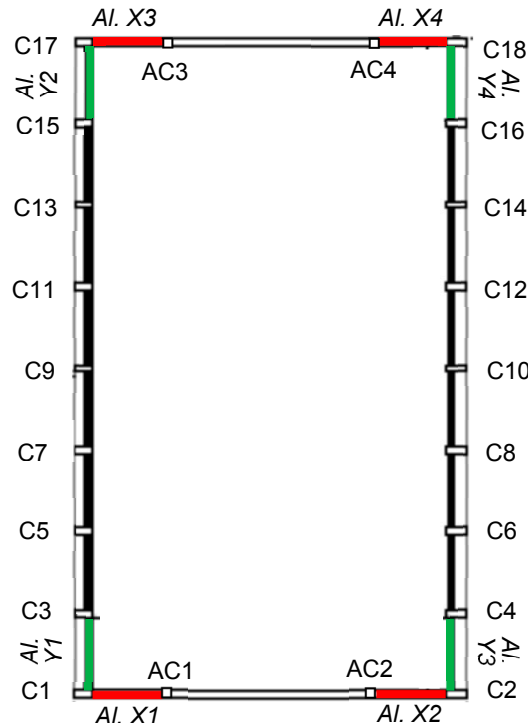
541



553 **Figure 10.** Installation details of the dissipative bracing system in the case study building.

554 *5.2 Application of the Design Method to the Case Study Building*

555 As shown in the building plan in Figure 11, the dissipative braces are placed in four alignments  
556 parallel to X (named Al. X1 through Al. X4) and four alignments parallel to Y (Al. Y1–Al. Y4). The  
557 latter are constituted by pairs of adjacent columns (C1–C3 – Al. Y1, C15–C17 – Al. Y2, C2–C4 – Al.  
558 Y3, C16–C18 – Al. Y4). Concerning the X-parallel alignments, because the beam span is about 11 m  
559 long, four additional RC columns with mutual section 250×250 mm×mm, named AC1 through AC4  
560 in Figure 11, are built at a distance of 3 m from the corner columns prior to mounting the bracing  
561 members.



579 **Figure 11.** Positions of the dissipative bracing system alignments in plan.

580 Based on the results of the assessment analysis reported in Section 4, the dissipaters are  
581 incorporated on the second level only, since the first level drifts computed in current conditions can  
582 produce only a marginal activation even of the smallest FV devices in standard manufacturing.

583 Consequently, traditional non dissipative braces are installed on the first level in the same four plus  
 584 four vertical alignments, so as to provide the necessary structural continuity with the dissipative  
 585 bracing system placed on the second level, as illustrated in the elevation view of Figure 10, but  
 586 without adding any further supplemental damping contribution. The application of steps 2 through  
 587 4 of the design procedure is summarized below for X and Y directions.

588 X direction – Lack of bending moment strength in columns

589 Step 2. The verification analysis in current conditions highlights that the most critical response  
 590 parameters in X direction are the bending moments around Y (i.e.  $M_Y$ ) in the first level columns, with  
 591 the highest unsafe conditions checked in the four corner columns. By referring to the nomenclature  
 592 in Section 2.1, the maximum moment  $M_{Y,c}^a$  corresponding to the peak response point in Figure 9c,  
 593 and associated with the concurrent axial force  $N_c=104$  kN mentioned above, is equal to 398.7 kNm.  
 594 The elastic limit moment  $M_{Y,c}^e$  of the corner columns around the Y axis is equal to 224.8 kNm. Thus,  
 595 the stress reduction factor  $\alpha_s = \alpha_{MY}$  of the critical members in X direction results as follows:

$$596 \quad \alpha_s = \alpha_{MY} = \frac{M_{Y,c}^a}{M_{Y,c}^e} = 1.77 \quad (24)$$

597 Passing from the member to the frame structure level (equivalent to the frame structure storey for  
 598 this case study building), since all columns have the same cross section,  $\alpha_F$  ratio coincides with  $\alpha_{MY}$ :

$$599 \quad \alpha_F = \alpha_{MY} = 1.77 \quad (25)$$

600 Step 3. Based on this value, the equivalent viscous damping ratio of the set of spring-dampers  
 601 to be installed on the second level is evaluated by means of relation (14), obtaining:

$$602 \quad \xi_{eq}(\alpha_F) = \frac{2}{\pi} \frac{(\alpha_F - 1)}{\alpha_F} = 0.277 \quad (26)$$

603 Step 4. The  $E_D$  energy dissipation capacity of the spring-dampers is calculated by expression (18).  
 604 The elastic limit values of the level shear  $F_e$  (i.e. the sum of the elastic limit shear forces of columns)  
 605 and the first inter-level drift  $ILD_e$  (replacing  $ID_e$  in this case) computed in X direction, named  $F_{e,X}$  and  
 606  $ILD_{e,1L,X}$ , are equal to 969 kN and 22 mm, respectively. Introducing these values, as well as  $\alpha_F$  and  
 607  $\xi_{eq}(\alpha_F)$  values given by (25) and (26), in (18), the following  $E_D$  estimate is derived:

$$608 \quad E_D(\alpha_F) = 2\pi\alpha_F F_{e,X} \xi_{eq}(\alpha_F) ILD_{e,1L,X} = 65.6 \text{ kJ} \quad (27)$$

609 Dividing  $E_D$  by the number of spring-dampers placed in X, the minimum energy dissipation  
 610 capacity  $E_{D,X,d}$  to be assigned to each of the 8 devices in order to reach the target performance at the  
 611 MCE results as follows:  $E_{D,X,d}=8.2$  kJ. The spring-damper type with the nearest nominal energy  
 612 dissipation capacity,  $E_n$ , to  $E_{D,X,d}$  has the following mechanical properties, drawn from the

613 manufacturer's catalogue [22]:  $E_n=9$  kJ; stroke  $s_{max}=\pm 30$  mm; damping coefficient  $c=9.9$  kN(s/mm) $^\gamma$ ,  
 614 with  $\gamma=0.15$ ;  $F_0=17$  kN; and  $k_2=1.74$  kN/mm.

615 Y direction – Lack of bending moment strength in columns and excessive inter-level drift

616 Step 2. The critical response parameters in Y direction are represented by the bending moments  
 617 around X ( $M_X$ ) in the second level columns, with the highest unsafe conditions checked in the four  
 618 corner columns too, and the second inter-level drifts. The maximum moment  $M_{X,c}^a$ , corresponding  
 619 in this case to the peak response point in Figure 9d, is equal to 174.2 kNm, whereas the elastic limit  
 620 moment  $M_{X,c}^e$  is equal to 84.2 kNm. Therefore, the stress reduction factor  $\alpha_s = \alpha_{MX}$  of the critical  
 621 members in Y direction is:

$$622 \quad \alpha_s = \alpha_{MX} = \frac{M_{X,c}^a}{M_{X,c}^e} = 2.07 \quad (28)$$

623 and thus:

$$624 \quad \alpha_F = \alpha_{MX} = 2.07 \quad (29)$$

625 The deformation-related reduction factor  $\alpha_d$  given by (19) is calculated for  $ILD_{max}$  (replacing  
 626  $ILD_{max}$ ) and  $ILD_e$  (replacing  $ILD_e$ ) values computed on the second level in Y direction, named  $ILD_{max,2L,Y}$ ,  
 627  $ILD_{e,2L,Y}$  in the following.  $ILD_{max,2L,Y}$  – corresponding to the  $ILD_{r,max}$  value of 1.69% mentioned in  
 628 Section 4.2 – is equal to 72.7 mm, and  $ILD_{e,2L,Y}$  to 36.8 mm, yielding:

$$629 \quad \alpha_d = \frac{ILD_{max,2L,Y}}{ILD_{e,2L,Y}} = 1.98 \quad (30)$$

630 Step 3. The equivalent viscous damping ratio is calculated in this case by referring both to  $\alpha_F$  and  
 631  $\alpha_d$ , using expressions (14) and (20), respectively:

$$632 \quad \xi_{eq}(\alpha_F) = \frac{2}{\pi} \frac{(\alpha_F - 1)}{\alpha_F} = 0.33 \quad (31)$$

$$633 \quad \xi_{eq}(\alpha_d) = \frac{2}{\pi} (\alpha_d - 1) = 0.624 \quad (32)$$

634 Step 4. Named  $F_{e,Y}$  the elastic limit level shear in Y direction, by applying the  $E_D$  energy  
 635 dissipation capacity expressions (18) and (21), the following  $E_D$  estimates are obtained:

$$636 \quad E_D(\alpha_F) = 2\pi\alpha_F F_{e,Y} \xi_{eq}(\alpha_F) ILD_{e,2L,Y} = 100.8 \text{ kJ} \quad (33)$$

$$637 \quad E_D(\alpha_d) = 2\pi F_{e,Y} \xi_{eq}(\alpha_d) ILD_{e,2L,Y} = 92.1 \text{ kJ} \quad (34)$$

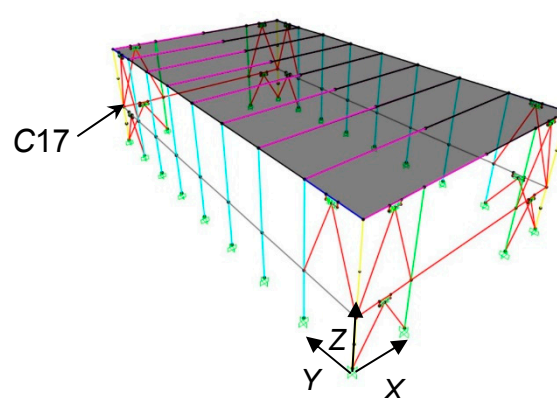
638 where  $F_{e,Y}=638$  kN.

639 By comparing  $\xi_{eq}(\alpha_F)$  with  $\xi_{eq}(\alpha_d)$ , and  $E_D(\alpha_F)$  with  $E_D(\alpha_d)$ , it can be observed that the relevant  
 640 ratios are rather different. Indeed:  $\xi_{eq}(\alpha_d)/\xi_{eq}(\alpha_F)=1.89$ ,  $E_D(\alpha_F)/E_D(\alpha_d)=1.1$ . This is due to the fact that,  
 641 consistently with the general  $\xi_{eq}$  expression (5), the damping coefficient depends on  $E_e$ , and thus on  
 642 the elastic properties of the device, which are a function of the maximum displacement and force  
 643 reached in the time-history response, in addition to the hysteretic response. On the other hand, the  
 644 dissipated energy  $E_D$  is only determined by the area covered by the response cycles, which identifies  
 645 it as a more stable and reliable parameter for the design of the FV devices.  $\xi_{eq}$  is only a useful synthetic  
 646 measure of their limit damping capacity.

647 The design process is completed by referring to the largest of the energy values,  $E_D(\alpha_F)$ ,  $E_D(\alpha_d)$ ,  
 648 i.e.  $E_D(\alpha_F)=100.8$  kJ. Similarly to X direction, the minimum energy dissipation capacity of each of the  
 649 8 devices placed in Y,  $E_{D,Y,d}$ , in order to achieve the target performance at the MCE is obtained by  
 650 dividing  $E_D(\alpha_d)$  by the number of spring-dampers:  $E_{D,Y,d}=12.6$  kJ. The device with the nearest nominal  
 651 energy dissipation capacity to  $E_{D,Y,d}$  has the following mechanical properties:  $E_n=14$  kJ; stroke  $s_{max}=\pm 40$   
 652 mm; damping coefficient  $c=14.16$  kN(s/mm) $^\gamma$ , with  $\gamma=0.15$ ;  $F_0=28$  kN; and  $k_2=2.1$  kN/mm.

### 653 5.3 Numerical Verification of the Retrofit Solution

654 A perspective view of the model including the dissipative bracing system is displayed in Figure  
 655 12. The modal analysis carried out in retrofitted conditions confirms the sequence of modes computed  
 656 in current state, with differences on periods and EMMs lower than 10%, as a consequence of the small  
 657 stiffening effect of this technology. Periods and EMMs of the two first horizontal translational modes  
 658 along X and Y pass to 0.83 s (Y) and 0.32 s (X), and to 79.5% (Y) and 88.1% (X); periods and EMMs of  
 659 the fourth and fifth mode, translational along X and Y, to 0.25 s (Y) and 0.105 s (X), and to 20.3% (Y)  
 660 and 11.7% (X). Relevant summed modal masses are nearly equal to 100% along both axes, in this case  
 661 too. The third and sixth mode, rotational around Z, have periods of 0.33 s and 0.037 s, and EMM equal  
 662 to 84.9% and 13.8%, giving a summed modal mass of 98.7%.

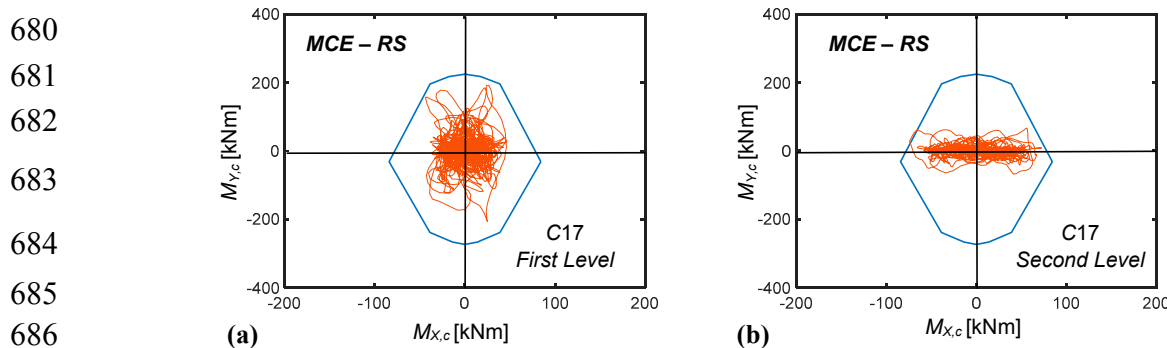


663  
 664  
 665  
 666  
 667  
 668  
 669  
 670 **Figure 12.** View of the finite element model incorporating the dissipative bracing system.

671 The results of the time-history verification analyses in rehabilitated configuration are  
 672 synthesized in Figures 13 through 16, all referred to the response induced by the most demanding of  
 673 the seven groups of input ground motions scaled at the MCE level. The  $M_x-M_{Yc}$  interaction curves  
 674 of the first and second level base sections of column C17, plotted in Figure 9c,d above for the original  
 675 structure, are duplicated in Fig. 13 in retrofitted conditions. The two graphs show that the dissipative  
 676 action of the protective system allows confining the interaction curves within the biaxial moment safe

677 domain, reducing the maximum  $M_{Yc}$  (Figure 13a) and  $M_{Xc}$  (Figure 13b) moments nearly by the  
 678 targeted  $\alpha_{MY}$  and  $\alpha_{MX}$  factors of 1.77 and 2.07, as given by (24) and (29).

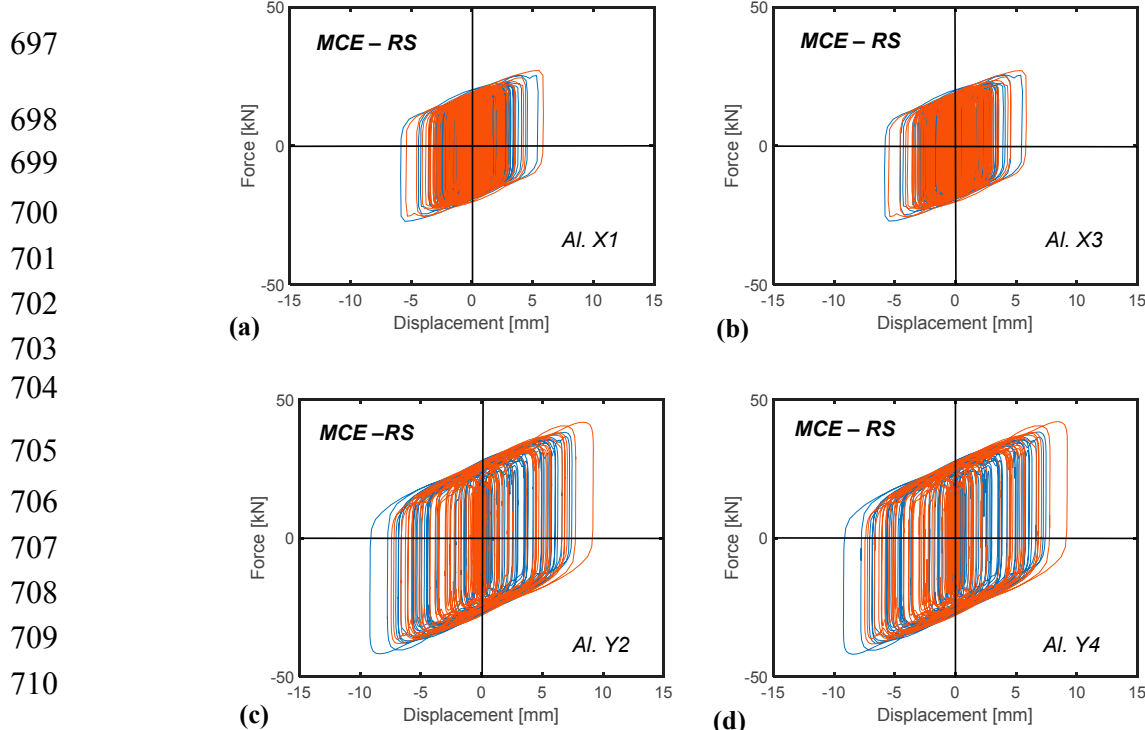
679



687 **Figure 13.** Retrofitted structure (RS).  $M_{X,c}$ – $M_{Y,c}$  biaxial moment interaction curves at the base section of  
 688 column C17 on first level (a) and second level (b) obtained from the most demanding MCE-scaled group  
 689 of accelerograms.

690 The response cycles of the pairs of spring-dampers situated along the diagonally opposite  
 691 vertical alignments *Al. X1*, *Al. X3*, and *Al. Y2*, *Al. Y4* are visualized in Figure 14. The cycles exhibit  
 692 peak displacements equal to 6.3 mm (*Al. X1*, *Al. X3*) and 8.8 mm (*Al. Y2*, *Al. Y4*), far below the  
 693 available stroke limits of  $\pm 30$  mm (in X) and  $\pm 40$  mm (in Y) mentioned above. Furthermore, the  
 694 response of the devices placed in *Al. X1* and *Al. X3* are nearly coincident, and the same occurs for the  
 695 devices situated in *Al. Y2* and *Al. Y4*, highlighting that torsion effects in plan are virtually null.

696



712 **Figure 14.** Retrofitted structure (RS). Response cycles of the spring-damper pairs installed in *Al. X1* (a), *Al. X3*  
 713 (b), *Al. Y2* (c) and *Al. Y4* (d) vertical alignments obtained from the most demanding MCE-scaled group of  
 714 accelerograms.

715 The energy time-histories graphed in Figure 15, where  $E_I$  and  $E_D$  denote the total input and dissipated  
 716 energies, and  $E_{I,X}$ ,  $E_{D,X}$ ,  $E_{I,Y}$ ,  $E_{D,Y}$  the relevant portions in  $X$  and  $Y$ , show  $E_{D,X}$ ,  $E_{D,Y}$  values of 66.9 kJ and 101.9  
 717 kJ, which differ only by 2% and 1% from the corresponding  $E_D(\alpha_F)$  estimates (27) and (33), respectively.

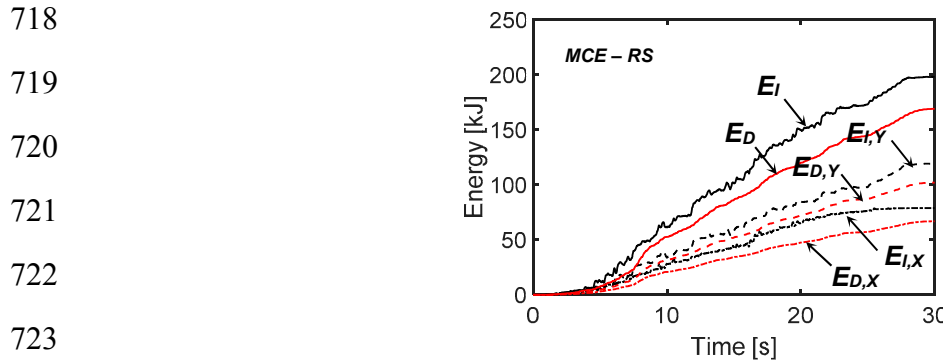


**Figure 15.** Retrofitted structure (RS). Energy time-histories obtained from the most demanding MCE-scaled group of accelerograms.

726 Furthermore, practically identical values of the  $E_D/E_I$  ratio are found in  $X$  and  $Y$ , namely:  $E_{D,X}/E_{I,X}=0.85$ ;  
 727  $E_{D,Y}/E_{I,Y}=0.855$ , identifying a well balanced energy dissipation demand in the two directions.

728 The roof top displacement time-histories illustrated in Figure 16 show a reduction factor on the peak values  
 729 equal to about 2.3 ( $X$ ) and 2.2 ( $Y$ ) when passing from current (CS) to retrofitted (RS) conditions. In the most  
 730 deformable direction  $Y$  this corresponds to a drop of the second level drift from 72.7 mm to 33.8 mm, i.e. below  
 731 the corresponding elastic limit value  $ILD_{e,2L,Y}=36.8$  mm, as targeted in the design.

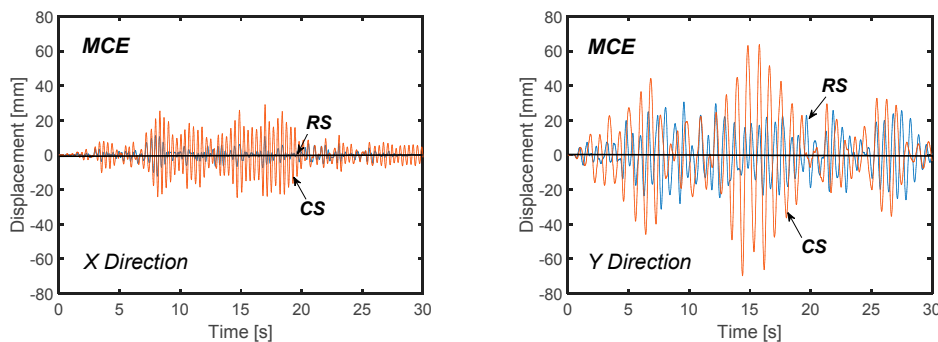


**Figure 16.** Roof top displacement time-histories obtained from the most demanding MCE-scaled group of accelerograms.

## 740 5. Conclusions

741 The energy-based design criterion formulated in this study for the seismic retrofit of frame  
 742 buildings by means of dissipative bracing technologies does not require any preliminary evaluation  
 743 of the input energy demand on the original structure. At the same time, the most critical response  
 744 parameters in current conditions — the reduction of which within the boundary of relevant safe  
 745 domains (in case of lack of strength), or below limits preventing damage to structural and non-  
 746 structural elements (in case of excessive lateral displacements) — are evaluated by a conventional  
 747 elastic finite element analysis. Both aspects of the initializing step of the sizing procedure allow  
 748 simplifying the design of supplemental damping-based retrofit solutions, which can be useful  
 749 especially for professional engineers not familiar with seismic energy computation and the  
 750 development of non-linear time-history analyses.

751 The criterion was detailed here for relatively stiff structures, i.e. with fundamental translational  
 752 vibration period in original conditions below 0.8 s, where the retrofit design objectives can be met by

753 added damping, with a marginal role of supplemental stiffness. This prompted to select the bracing  
754 systems that incorporate FV spring-dampers as protective devices, because they provide a moderate  
755 contribution to the lateral stiffness of the retrofitted structures. However, the procedure can be  
756 extended with little modifications to dissipative bracing technologies that significantly increase the  
757 translational stiffness too, like the systems including metallic dampers, which will be the subject of a  
758 further step of the study.

759 The demonstrative application to the considered case study structure allowed checking the  
760 quick sizing characteristics of the design criterion, even when stress state-related and drift-related  
761 deficiencies are both found in the original structure (as occurs in Y direction of the gym building).  
762 Furthermore, the values of the equivalent damping coefficient ratio calculated as a function of the  
763 reduction factors  $\alpha_F$ ,  $\alpha_d$  relevant to stress states and drifts, using formulas (14) and (20), respectively,  
764 resulted to be notably different. On the other hand, a slight difference was found between the  
765 corresponding energy dissipation measures,  $E_D(\alpha_F)$  and  $E_D(\alpha_d)$ . This identified  $E_D$  as a more stable  
766 and reliable design parameter, as compared to  $\xi_{eq}$ , consistently with the fact that  $E_D$  is only determined  
767 by the area covered by the response cycles of the dissipaters. This was also confirmed by the fact that  
768 the  $E_D$  values in X and Y computed from the time-history verification analysis were very similar to  
769 the  $E_D(\alpha_F)$  estimates.

770 As targeted in the retrofit design, the incorporation of the protective system in the gym building  
771 allows reaching an elastic and safe response of all members, as well as constraining the inter-level  
772 drifts below the Immediate Occupancy drift limit, up to the MCE, starting from a rather poor  
773 performance in original conditions.

774 **Acknowledgments:** The study reported in this paper was sponsored by the Italian Department of Civil  
775 Protection within the ReLUIS-DPC Project 2014/2018, Research Line 6: Isolation and Dissipation. The author  
776 gratefully acknowledge this financial support.

777 **Conflicts of Interest:** The author declares no conflict of interest.

## 778 References

- 779 1. Foti, D.; Bozzo, L.; Lopez-Almansa, F. Numerical efficiency assessment of energy dissipators for seismic  
780 protection of buildings. *Earthquake Engineering and Structural Dynamics*, **1998**, *27*(6), 543–556, DOI:  
781 10.1002/(SICI)1096-9845(199806)27:6.
- 782 2. Aiken, I.D.; Nims, D.K.; Whittaker, A.S.; Kelly, J.M. Testing of passive energy dissipation systems.  
*Earthquake Spectra*, **1993**, *9*(3), 335–370, DOI: 10.1193/1.1585720.
- 783 3. Sorace, S.; Terenzi, G. Seismic protection of frame structures by fluid viscous damped braces. *Journal of  
784 Structural Engineering, ASCE*, **2008**, *134*(1), 45–55, DOI: 10.1061/(ASCE)0733-9445(2008)134:1(45).
- 785 4. Constantinou, M.C.; Symans, M.D. Experimental study of seismic response of buildings with supplemental  
786 fluid dampers. *Journal of the Structural Design of Tall Buildings*, **1993**, *2*(2), 93–132, DOI:  
787 10.1002/tal.4320020203.
- 788 5. Ramirez, O.M.; Constantinou, M.C.; Kircher, C.A.; Johnson, M.W.; Chrysostomou, C.Z. Validation of the  
789 2000 NEHRP provisions' equivalent lateral force and modal analysis procedures for buildings with  
790 damping systems. *Earthquake Spectra*, **2003**, *19*(4), 981–999, DOI: 10.1193/1.1622392.
- 791 6. Whittaker, A.; Constantinou, M.; Ramirez, O.; Johnson, M.; Chrysostomou, C. Equivalent lateral force and  
792 modal analysis procedures for the 2000 NEHRP provisions for buildings with damping systems. *Earthquake  
793 Spectra*, **2003**, *19*(4), 959–980, DOI: 10.1193/1.1622391.
- 794 7. Hanson, R.D.; Soong, T.T. *Seismic design with supplemental energy dissipation devices*. Publication MNO-8  
795 EERI–Earthquake Engineering Research Center: Oakland, CA, 2001.
- 796 8. Soong, T.T.; Spencer, B.F. Supplemental energy dissipation: state-of-the-art and state-of-the-practice.  
*Engineering Structures*, **2002**, *24*(3), 243–259, DOI: 10.1016/S0141-0296(01)00092-X.
- 797 9. Ramirez, O.M.; Constantinou, M.C.; Whittaker, A.S.; Kircher, C.A.; Chrysostomou, C.Z. Elastic and Inelastic  
798 Seismic Response of Buildings with Damping Systems. *Earthquake Spectra*, **2002**, *18*(3), 531–547, DOI:  
799 10.1193/1.1509762.
- 800 10. Christopoulos, C.; Filiatrault, A. *Principles of passive supplemental damping and seismic isolation*. IUSS PRESS:  
801 Pavia, Italy 2006; ISBN: 88-7358-037-8.

804 11. ASCE/SEI 41-06. *Seismic rehabilitation of existing buildings*. American Society of Civil Engineers – Structural  
805 Engineering Institute: Reston, VA, 2006.

806 12. ASCE 7-10. *Minimum design loads for buildings and other structures*. American Society of Civil Engineers:  
807 Reston, VA, 2010.

808 13. Silvestri, S.; Gasparini, G.; Trombetti, T. A five-step procedure for the dimensioning of viscous dampers to  
809 be inserted in building structures. *Journal of Earthquake Engineering*, **2010**, *14*(3), 417-447, DOI:  
810 10.1080/13632460903093891.

811 14. Palermo, M.; Muscio, M.; Silvestri, S.; Landi, L.; Trombetti, T. On the dimensioning of viscous dampers for  
812 the mitigation of the earthquake-induced effects in moment-resisting frame structures. *Bulletin of Earthquake  
813 Engineering*, **2013**, *11*(6), 2429-2446, DOI: 10.1007/s10518-013-9474-z .

814 15. Bergami, A.V.; Nuti, C. A design procedure of dissipative braces for seismic upgrading structures.  
815 *Earthquake and Structures*, **2013**, *4*(1), 85-108, ISSN: 20927614.

816 16. Mazza, F.; Mazza, M.; Vulcano, A. Displacement-based seismic design of hysteretic damped braces for  
817 retrofitting in-elevation irregular r.c. framed structures. *Soil Dynamics and Earthquake Engineering*, **2015**, *69*,  
818 115-124, DOI: 10.1016/j.soildyn.2014.10.029.

819 17. Mazza, F. Comparative study of the seismic response of RC framed buildings retrofitted using modern  
820 techniques. *Earthquake and Structures*, **2015**, *9*(1), 29-48, DOI: 10.12989/eas.2015.9.1.029.

821 18. Sorace, S.; Terenzi, G.; Fadi, F. Shaking table and numerical seismic performance evaluation of a fluid  
822 viscous-dissipative bracing system. *Earthquake Spectra*, **2012**, *28*(4), 1619-1642, DOI: 10.1193/1.4000083.

823 19. Sorace, S.; Terenzi, G.; Mori, C. Passive energy dissipation-based retrofit strategies for R/C frame water  
824 storage tanks. *Engineering Structures*, **2016**, *106*, 385-398, DOI: 10.1016/j.engstruct.2015.10.038.

825 20. Sorace, S.; Terenzi, G.; Licari, M. Traditional and viscous dissipative steel braced top addition strategies for  
826 a R/C building. *International Journal of Structural Engineering*, **2015**, *6*(4), 332-353, DOI:  
827 10.1504/IJSTRUCTE.2015.072472.

828 21. Jarret SL. Shock-control technologies. URL <http://www.introini.info>; 2017.

829 22. Italian Council of Public Works. *Technical Standards on Constructions*. Italian Council of Public Works: Rome,  
830 Italy, 2008 [in Italian].

831 23. Italian Council of Public Works. *Commentary on the Technical Standards on Constructions*. Italian Council of  
832 Public Works: Rome, Italy, 2009 [in Italian].

833 24. Pieraccini, M.; Parrini, F.; Fratini, M.; Atzeni, C.; Spinelli, P.; Micheloni, M. Static and dynamic testing of  
834 bridges through microwave interferometry. *NDT and E International*, **2007**, *40*(3), 208-214, DOI:  
835 10.1016/j.ndteint.2006.10.007

836 25. Allend, D.E. Safety criteria for the evaluation of existing structures. In: Proceedings of IABSE Colloquium  
837 - Remaining Structural Capacity, Copenhagen, Denmark, March, 17-19 March, 1993.

838 26. SAP2000NL. *Theoretical and users' manual. Release 18.05*. Computers & Structures Inc.: Berkeley, USA, 2017.

839 27. Vanmarcke, E.H.; Fenton, G.A.; Heredia-Zavoni, E. *SIMQKE-II – Conditioned earthquake ground motion  
840 simulator: User's manual, version 2.1*. Princeton University: Princeton, USA, 1999; URL  
841 <http://nisee.berkeley.edu/documents/SW/SIMQKE-II-V2-1.pdf>.

842 28. EN 1998-4. Eurocode 8: Design of structures for earthquake resistance - Part 1: general seismic rules. *Seismic  
843 Actions and Rules for Buildings*. European Committee for Standardisation: Brussels, Belgium, 2003.

844 29. Terenzi G. Effetti dissipativi nell'isolamento sismico. PhD Thesis, University of Florence, Italy, 1996 [in  
845 italian].

846 30. Terenzi, G. Dynamics of SDOF systems with nonlinear viscous damping. *Journal of Engineering Mechanics,  
847 ASCE*, **1999**, *125*(8), 956-963, DOI: 10.1061/(ASCE)0733-9399(1999)125:8(956).

848 31. Sorace, S.; Terenzi, G. Non-linear dynamic modelling and design procedure of FV spring-dampers for base  
849 isolation. *Engineering Structures*, **2001**, *23*(12), 1556-1567, DOI: 10.1016/S0141-0296(01)00063-3.

850 32. Sorace, S.; Terenzi, G. Motion control-based seismic retrofit solutions for a R/C school building designed  
851 with earlier Technical Standards. *Bulletin of Earthquake Engineering*, **2014**, *12*, 2723-2744, DOI:  
852 10.1007/s10518-014-9616-y.

853